

# Multi-Exposure Image Fusion based on Window Segmentation and a Laplacian Pyramid for Chip Package Appearance Quality Detection

Fei Hao<sup>1</sup>, Jiatong Song<sup>2</sup>, Jiahao Sun<sup>3</sup>, Yang Fu<sup>4</sup>

Kangni Industrial Technology Research Institute, Nanjing Institute of Technology, Nanjing, China

**Abstract**—A heterogeneous material image enhancement method based on multi-exposure image fusion is proposed to address the problem of obtaining high-quality images from the single imaging of chips containing two extremely different reflectivity materials. First, a multi-exposure image fusion algorithm based on window segmentation and Laplacian pyramid fusion is proposed. Then, orthogonal experiments are used to optimize the parameters of the imaging system. Next, a method based on information entropy and average gray intensity is utilized to calculate the imaging exposure times of two heterogeneous materials, and two exposure time ranges are obtained that are appropriate for regions with high and low reflectivity. Finally, the subjective and objective experimental evaluations are conducted after the multi-exposure image set has been established. The results show that the fused image has a good visual effect, the information entropy is 6.29, and the average gray intensity is 131.56. In addition, time consumption is reduced by an average of 20.3% compared to the Laplace pyramid strategy. The heterogeneous material enhancement method based on multi-exposure image fusion proposed in this paper is effective and deserving of further research and application.

**Keywords**—Image fusion; multi-exposure; Laplacian pyramid; window segmentation; chip package

## I. INTRODUCTION

Chip defect detection typically includes size measurement, character detection, stain detection and pin defect detection [1]. It is found that because chips in ordinary cameras contain both high reflectivity metal and low reflectivity black plastic, they cannot capture all information through a single image when collecting images [2]. At present, there are devices for directly acquiring high dynamic images [3], but such hardware devices have high cost and few applications, so software algorithm enhancement methods are widely considered instead.

This paper aims to propose a new multi-exposure image fusion method to improve the image quality of an object composed of a variety of materials with very different reflectivity. The main contributions are as follows:

- An image fusion method based on window segmentation and Laplace pyramid was proposed.
- The optimal imaging parameters of the established machine vision system were determined by the orthogonal experiments.

- A strategy for determining the optimal exposure time based on information entropy and average gray intensity was proposed.
- The experimental results show that the image information entropy and average gray intensity of the fused image by our method were 6.29 and 131.56 respectively and the time was averagely reduced by about 1.26 s.

The rest of this paper is organized as follows: the first section is the introduction. The second section reviews the related work in multi-exposure image fusion. The third section describes the image fusion algorithm. In the fourth section, the main factors affecting the imaging quality are determined by orthogonal testing, and the level of the influencing factors is optimized. In the fifth section, through information entropy and average gray intensity, the optimal exposure time for imaging objects with multiple heterogeneous materials is determined. The sixth section discusses the experiment and the analysis of the results. Finally, conclusions are presented.

## II. RELATED WORKS

Currently, image quality enhancement algorithms are divided into two categories. One is based on single source image enhancement [4], which primarily use the spatial domain and transform domain to enhance a single image to improve the problems of detail loss and uneven lighting. Common spatial methods include grayscale transformation, histogram equalization, contrast enhancement and other methods [5]. Among them, the histogram equalization method is the most commonly used airspace method. The global histogram equalization map is highly efficient, but the enhanced image will easily lose details. Therefore, Celik [6] adopted the local histogram equalization algorithm based on information entropy to solve the problem of image texture loss. The local histogram equalization map can enhance the local details of the image but lacks global integrity. Wavelet transform [7], discrete wavelet transform [8], stationary wavelet transform [9] and other transform domain methods distinguish the basic information and detailed information of the image and perform multi-exposure image fusion. At present, the transform domain algorithm based on the wavelet transform can achieve the effect of enhancing the image [10]. Such methods can enhance the details while taking into account the global whole but also magnify the noise in the image. Therefore, the final result of the single source image enhancement method experiences

noise and loss of detail, which is typically accepted in the field of natural images but is not suitable for size measurement and defect detection.

The other category is image fusion based on multi-source images. Image fusion refers to obtaining different image sequences of the same scene with imaging sensors and combining the details and complementary information of the image sequence to obtain a rich and comprehensive image [11]. Multi-Exposure Fusion (MEF) is one of the branches derived from image fusion; that is, it fuses multiple images with different exposures in the same scene into a new image, preserving the brightest and darkest details in the scene [12]. From the perspective of image decomposition, multi-exposure image fusion can be divided into pixel-based and image block-based fusion methods. Goshtasby [13] first proposed image block-based fusion and calculated the information entropy to select the best image block for fusion, but there was some distortion in the results. Qin Lyu used nonuniform triangulation to segment images [14]. T Prabhakara Rao performed feature-level image fusion based on contour blocking, improved the distortion and played a crucial role in developing its subsequent feature extraction and detection [15]. Compared with the method of nonuniform division of images, the fusion algorithm speed block based on uniform division of image blocks is more suitable for the application of industrial detection occasions, but it mainly emphasizes the selection of the optimal block of the image sequence, which frequently results in issues with discontinuous images and obvious stitching traces. In contrast, Mertens [16] proposed a pixel-based multi-exposure fusion method, which can make up for the shortcomings of discontinuous images but has a high computational complexity and low efficiency. An extremely critical method in pixel-based image fusion is pyramid decomposition [17], which constructs an image pyramid from the input image, adds a weight matrix, and finally combines the two to obtain the final fusion result. Ashish et al. adopted multiresolution fusion based on a Laplacian pyramid [18], measured by entropy and contrast, which is characterized by seamless fusion and excellent improved details. Zhong Qu and others improved pyramid decomposition and applied it to image fusion, improving the common artifact problem of multi-exposure fusion [19] and retaining more local details. The pyramid algorithm can typically preserve good image edges and textures, but the processing time is generally very long. The fusion method based on image blocks can greatly improve the computational efficiency and remove random noise. Therefore, it is expected that combining the pyramid algorithm with the image block algorithm will allow the fused image to maintain better details and improve the operational efficiency of the algorithm.

The optimal exposure time should be primarily determined according to the material characteristics of a specific object for developing the image fusion methods. The image gradient was employed in the fusion method proposed by Turgut et al. [20]. Image information entropy was adopted by Kataoka et al. as the only indicator to determine the exposure time for image fusion [21]. Camera response curve was uniquely selected and used for exposure fusion by Zhang et al. [22]. Thus it can be seen that the common indicators of exposure fusion include

image gradient, image information entropy and camera response curve, and they were used singly at present. However, these above methods may be invalid and inaccurate for objects with multi-materials. Therefore, this paper will also explore a new multivariate strategy to determine the optimal exposure time for imaging objects with multi-materials.

### III. MULTI-EXPOSURE IMAGE FUSION METHOD

#### A. Image Fusion Algorithm based on Laplacian Pyramid

The source image  $G_0$  undergoes multiple Gaussian fuzzy filtering and downsampling operations and continuously reduces the image size to obtain an image sequence  $(G_0, G_1, G_2, \dots, G_N)$ . The Gaussian pyramid is obtained by arranging  $G_0$  at the bottom and  $G_N$  at the top. The essence of the Gaussian pyramid is the multiscale representation of the image signal, as shown in Formula (1). The Laplacian pyramid is obtained by up sampling and interpolation of the Gaussian pyramid [23], and the image sequence can be represented by  $(LP_0, LP_1, LP_2, \dots, LP_N)$ , as shown in Formula (2).

$$G_l(i, j) = \sum_{m=-2}^2 \sum_{n=-2}^2 w(m, n) G_{l-1}(2i+m, 2j+n) \quad (1)$$

where  $w(m, n)$  is a Gaussian convolution kernel with a fixed size.

$$\begin{cases} LP_l = G_l - G_{l+1}^* & 0 \leq l < N \\ LP_N = G_N & l = N \end{cases} \quad (2)$$

where  $G_{l+1}^*$  is calculated according to Formula (3):

$$G_l^* = 4 \sum_{m=-2}^2 \sum_{n=-2}^2 w(m, n) G_l\left(\frac{i+m}{2}, \frac{j+n}{2}\right) \quad (3)$$

For multi-exposure image fusion based on the Laplacian pyramid strategy, each layer of images were first processed in multiple Laplacian pyramids according to the strategy in Formula (4) to obtain the fused Laplacian pyramid image sequence, and then obtain the fused source image according to the method in Formula (5).

$$FLP_l = \sum_{k=1}^H \lambda_k \cdot (LP_l)_k \quad (4)$$

where  $H$  is the number of multi-exposure images,  $(LP_l)_k$  represents the  $l$ -th layer of the Laplacian pyramid decomposition image of the  $k$ -th image,  $\lambda_k$  is the weight coefficient corresponding to the  $k$ -th image, and  $FLP_l$  is the weighted fusion result of the  $l$ -th decomposition image of the  $H$  multi-exposure image.

$$\begin{cases} FG_N = FLP_N, & 0 \leq l < N \\ FG_l = FLP_l + FG_{l+1}^*, & 0 \leq l < N \end{cases} \quad (5)$$

In the formula,  $FG_l$  is the Laplacian pyramid decomposition image of layer  $l$  of the fused image, and  $FG_{l+1}^*$  is calculated according to Formula (3).

The image fusion based on the Laplacian pyramid strategy comprehensively uses the information of the source image at different spatial frequency levels. Compared with traditional fusion methods, there is no obvious stitching trace, but it also has the problem of long computing times.

**B. Multi Exposure Image Fusion Algorithm based on Window Segmentation**

Divide the  $H$  multiple exposure light source images evenly to obtain an image block with size  $m \times n$ . The  $j$ -th image block in the  $i$ -th source image is represented by  $A_{i,j}$ . Select an appropriate image quality evaluation index to quantize  $\{A_{i,j}\}$ , and select the optimal image block  $B_j$ . As shown in Formula (6), the fused image is finally obtained by "splicing" all the  $B_j$ . The basic process of the multi-exposure image fusion algorithm based on window segmentation is shown in Fig.1.

$$B_j = \text{Optimal}(\text{Indicator}(\{A_{i,j}\})) \quad (6)$$

In Formula (6),  $i = 1, 2, \dots, H$ ,  $j = 1, 2, \dots, M$ ,  $M$  is the number of image blocks,  $\text{Indicator}(\cdot)$  represents the quantitative evaluation function of image quality, and  $\text{Optimal}(\cdot)$  represents the optimization function.

Optimizing the exposure quality evaluation index of image blocks and the image block "splicing" algorithm are the core of the multi-exposure image fusion algorithm based on window segmentation. The uniform block-based fusion algorithm has high efficiency, but an inappropriate evaluation index and "splicing" algorithm easily lead to splicing traces. The nonuniform block fusion algorithm has the advantages of obvious edge information and large brightness width, but the efficiency of such methods is usually not high.

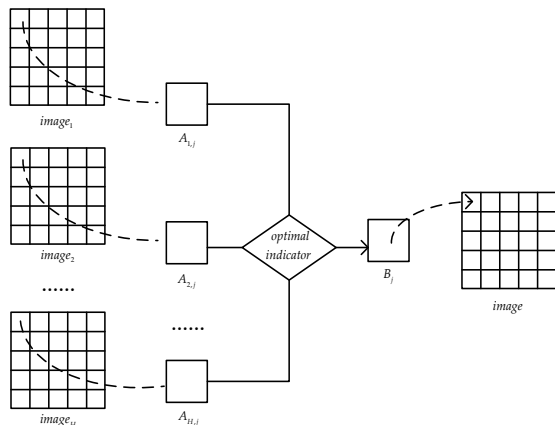


Fig. 1. Window segmentation fusion algorithm

**C. Image Fusion Algorithm based on Window Segmentation and Laplacian Pyramid**

The image fusion algorithm based on window segmentation and Laplacian pyramid combines the characteristics of high efficiency of window segmentation method and less stitching trace of Laplacian pyramid method. Same as window segmentation, first, the  $H$  source image is divided into  $M$  image blocks of size  $m \times n$ , and the  $j$ -th image block of the  $i$ -th source image is expressed as  $A_{i,j}$ . Then, the appropriate image quality evaluation index was selected to quantize and sort  $A_{i,j}$ , whose total quantity is  $M$ , and select the best  $N$  image blocks  $B_{k,j}$ . Then, the image fusion algorithm based on Laplace pyramid sideratio is adopted, and  $B_j$  is obtained by fusing  $N$  image blocks  $B_{k,j}$ . Finally, the fused image is obtained by "splicing" all the  $B_j$ . The basic process of the image fusion algorithm based on window segmentation and Laplacian pyramid is shown in Fig. 2.

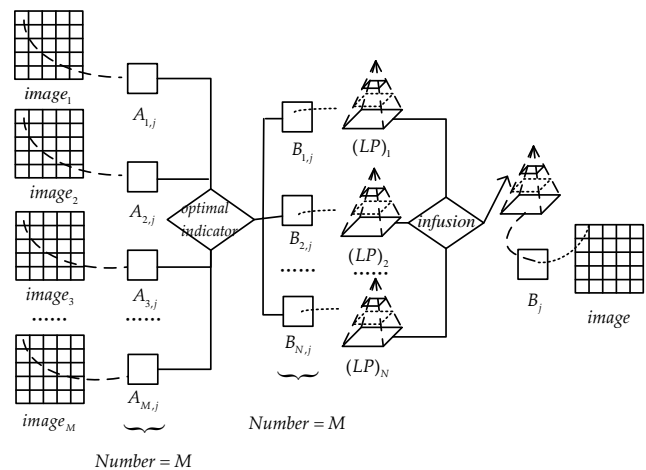


Fig. 2. Image fusion algorithm based on window segmentation and Laplacian pyramid

For vision systems, exposure time is not the only factor affecting the imaging system. Lighting, camera sensors and lenses are key factors that affect imaging. Therefore, before multi-exposure image fusion, this paper innovatively controls the image acquisition conditions and uses orthogonal experiments to optimize the parameters of the multi-exposure imaging system.

**IV. OPTIMAL PARAMETERS SELECTION METHOD FOR IMAGING SYSTEM AND ITS IMPLEMENTATION**

**A. Machine Vision System**

The experiment object of this paper is a semiconductor chip with a size of approximately  $4\text{mm} \times 4\text{mm}$ . A dual camera image acquisition system consisting of two telecentric lenses was built based on the characteristics of small distortion, as shown in Fig. 3.



Fig. 3. Binocular telecentric vision system

### B. Effect Factors of Imaging Quality and Its Levels

There are many factors that affect the image quality during the design of a machine vision system. Among them the ambient light, the artificial light and the camera gain are the three most concerned parameters. It is difficult to control the ambient light to reduce the impact on image quality and thus the dark rooms are typically used to isolate ambient light for image acquisition. The image quality will sharply vary with the light source intensity, light source direction and other illumination conditions. Therefore how to optimize arrangement of artificial lights to ensure the acquisition of high-quality images was studied. In the darkroom, a larger gain may be employed to have more luminous flux to increase the image brightness. However, a larger camera gain may amplify noise and thus reduce the image quality. Accordingly, how to determine the optimal camera gain is also very important. Therefore, in the orthogonal experimental design, the three factors of artificial light source, ambient light and gain must be analyzed to determine their optimal levels to provide stable experimental conditions for multi-exposure fusion research.

TABLE I. EFFECT FACTORS OF IMAGING QUALITY AND THEIR LEVELS

Levels	Factors		
	A	B	C
1	low	4.00	without a dark room
2	medium	5.00	with a dark room
3	high	6.00	/

The above three factors of imaging quality and their levels are tabulated in Table I. Factor A represents the artificial light and has three levels: low, medium and high light intensity of backlights. Factor B represents the gain and has three levels: 4.00 dB, 5.00 dB and 6.00 dB. Factor C represents the ambient light and has two levels: with or without a dark room.

### C. Image Quality Evaluation Indicators

An image collected by the machine vision system is an 8-bit single channel gray image. The image quality evaluation indicators include information entropy, average gray intensity, variance and average gradient, which are defined as follows:

#### 1) Information entropy $H$

$$H = \sum_{i=0}^{255} p_i \log p_i \quad (7)$$

where  $p_i$  represents the proportion of pixels whose gray value is  $i$  in the image.

#### 2) Average gray intensity $U$

$$U = \frac{\sum_{i=1}^m \sum_{j=1}^n I(i, j)}{m \times n} \quad (8)$$

where  $I(i, j)$  represents the gray intensity at  $(i, j)$  in the image.  $m$  and  $n$  are the size of the image along two coordinate directions.

#### 3) Variance $S$

$$S = \sqrt{\frac{\sum_{i=1}^m \sum_{j=1}^n (I(i, j) - U)^2}{m \times n}} \quad (9)$$

where  $I(i, j)$  represents the gray intensity at  $(i, j)$  in the image.  $m$  and  $n$  are the size of the image along two coordinate directions.  $U$  is the average gray intensity of the image.

#### 4) Average gradient $G$

$$G = \frac{1}{(m-1)(n-1)} \sum_{i=1}^{m-1} \sum_{j=1}^{n-1} \sqrt{\frac{1}{2} \left\{ [I(i+1, j) - I(i, j)]^2 + [I(i, j+1) - I(i, j)]^2 \right\}} \quad (10)$$

where  $I(i, j)$  represents the gray intensity at  $(i, j)$  in the image.  $m$  and  $n$  are the size of the image along two coordinate directions.

#### 5) Comprehensive evaluation indicator $W$

$$W = k \times H \times U \times S \times G \quad (11)$$

where  $k$  is a coefficient that is employed to normalize  $W$  to be between 0 and 1.

### D. Orthogonal Experiments and Results

The orthogonal experimental scheme was established as shown in Table II according to the orthogonal experimental design method.

TABLE II. ORTHOGONAL EXPERIMENTAL SCHEME L6 ( $3^2 \times 2$ )

Levels	Factors		
	A	B	C
1	1	1	1
2	2	1	2
3	3	2	1
4	1	2	2
5	2	3	1
6	3	3	2

According to the above orthogonal experimental scheme tabulated in Table II, the experiments were carried out with the left camera and the right camera. Six images were collected with the left camera, and the evaluation results of image quality are shown in Table III.

TABLE III. RESULTS OF 6 EXPERIMENTS WITH THE LEFT CAMERA

No.	Factors			Image Quality Evaluation Indicators				
	A	B	C	Information entropy	Average gray intensity	Variance	Average gradient	Comprehensive indicator
1	1	1	1	0.63	242.11	2802.76	0.21	0.908
2	2	1	2	0.61	241.61	3026.27	0.18	0.819
3	3	2	1	0.65	243.29	2431.72	0.23	0.860
4	1	2	2	0.61	241.56	3042.61	0.19	0.840
5	2	3	1	0.65	243.34	2411.14	0.23	0.893
6	3	3	2	0.63	242.62	2703.44	0.20	0.830

The results of orthogonal experiments were calculated by using the comprehensive indicator, whose values are tabulated in Table V.  $k_i$  is the sum of comprehensive indicators at the  $i$ -th level of factors and  $\bar{k}_i$  is the mean value of  $k_i$ .  $r$  is the range of  $k_i$ , and  $\sigma$  is the variance of  $k_i$ . The larger the range of a factor is, the more significant the impact of the factor on image quality. The larger the  $\bar{k}_i$  of a factor is, the more significant the impact of the level on image quality.

TABLE IV. RESULTS OF 6 EXPERIMENTS WITH THE RIGHT CAMERA

No.	Factors			Image Quality Evaluation Indicators				
	A	B	C	Information entropy	Average gray intensity	Variance	Average gradient	Comprehensive indicator
1	1	1	1	0.7000	241.280	2833.36	0.2400	1.1510
2	2	1	2	0.6600	240.640	3087.94	0.1900	0.9460
3	3	2	1	0.7100	243.070	2244.70	0.2600	1.0170
4	1	2	2	0.6700	240.530	3127.14	0.2000	0.9900
5	2	3	1	0.7100	243.050	2253.85	0.2800	1.0800
6	3	3	2	0.6900	242.260	2522.78	0.2200	0.9170

TABLE V. RESULTS OF ORTHOGONAL EXPERIMENTS BY COMPREHENSIVE EVALUATION INDICATORS

Camera	Factors	Evaluation Indexes							
		$k_1$	$k_2$	$k_3$	$\bar{k}_1$	$\bar{k}_2$	$\bar{k}_3$	$r$	$\sigma$
Left	A	1.748	1.712	1.690	0.8740	0.8560	0.8450	0.0290	0.00043
	B	1.727	1.700	1.723	0.8635	0.8500	0.8615	0.0135	0.00011
	C	2.661	2.489	/	0.8870	0.8300	/	0.0570	0.00162
Right	A	2.141	2.026	1.934	1.0705	1.0130	0.9670	0.1035	0.00538
	B	2.097	2.007	1.997	1.0485	1.0035	0.9985	0.0500	0.00152
	C	3.248	2.853	/	1.0827	0.9510	/	0.1317	0.00867

From Table III, Table IV and Table V, it can be seen that the ambient light has the greatest impact on image quality, camera gain has the smallest impact on image quality and backlight intensity has a moderate impact on image quality, i.e.,  $C > A > B$ . The image quality is the highest when the three influencing factors are set to the first level, i.e., the optimal parameter combination is  $C_1A_1B_1$ .

V. DETERMINATION OF EXPOSURE PARAMETERS BASED ON INFORMATION ENTROPY AND AVERAGE GRAY INTENSITY

A. Information Entropy-Exposure Time Model for Images of Single Material Object

The exposure time required in imaging is related to the reflectivity of the object surface. Dark areas with low reflectivity require longer exposure times. In contrast, bright areas with higher reflectivity require shorter exposure times. When imaging a single material object or an object with multiple materials but little difference in reflectivity, the relation curve of the information entropy of the acquired image to the exposure time is a downward parabola. The information entropy first increases with increasing exposure time. When the information entropy reaches the maximum value, it will decrease with increasing exposure time, as shown in Fig. 4.

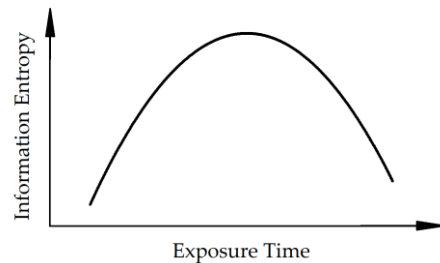


Fig. 4. Theoretical relationship between exposure time and image entropy

According to Fig. 4, when imaging a single material object or an object with multiple materials but little difference in reflectivity, the optimal exposure time can be set to  $[t_0 - t_1, t_0 + t_2]$ , where the exposure time is  $t_0$  and the information entropy is maximal.  $t_1$  and  $t_2$  are two positive numbers that are smaller than  $t_0$ .

B. Information Entropy-Exposure Time Model for Images of Multi-Material Objects

Different from single material object imaging, a multi-material object imaging has multiple peaks in its information entropy-exposure time curve, as shown in Fig. 5. The above method for determining the optimal exposure time cannot be directly used. Therefore, it is necessary to study the method of determining the optimal exposure time according to the characteristics of the information entropy-exposure time curve.

C. Determination of Optimal Exposure Time based on Information Entropy and Average Gray Intensity

The chip is composed of pins with high reflectivity and plastic packages with low reflectivity. As shown in Fig. 5, two peaks appear when the exposure time is 34200  $\mu s$  and 500000  $\mu s$ . If the selected exposure time is less than 34200  $\mu s$  or more than 500000  $\mu s$ , it will not be conducive to high-quality imaging of chips made of both materials. Therefore, the best exposure time must be between 34200  $\mu s$  and 500000  $\mu s$ .

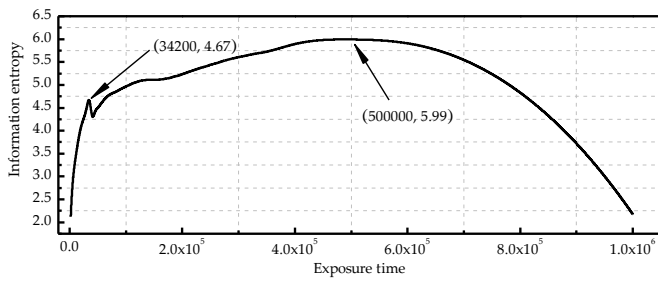


Fig. 5. Information entropy-exposure time curve of objects with two materials

The length of the above exposure time interval determined according to the information entropy is still relatively large. When collecting the pin image and the plastic package image, there is only one lower limit or upper limit of the exposure time. Therefore, the above interval needs to be further refined to obtain two subsections, which are applicable to collecting the pin image and the plastic package image. For this purpose, the relationship between the rate of the average gray intensity of images and the exposure time was analyzed. Fig. 6 and Fig. 7 show the first-order difference and the second-order difference of the model of image average gray intensity and exposure time, respectively.

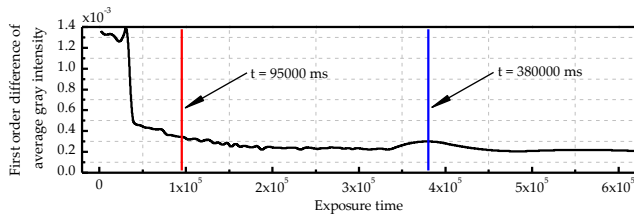


Fig. 6. First-order difference of image average gray intensity vs. exposure time

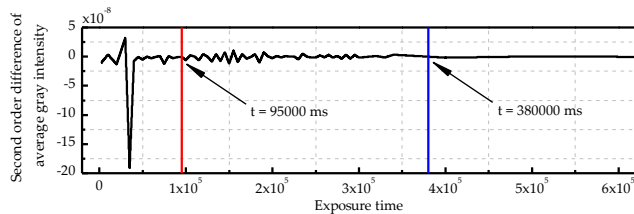


Fig. 7. Second-order difference of image average gray intensity vs. exposure time

Fig. 6 shows that when the exposure time is greater than 34200  $\mu\text{s}$  but less than 95000  $\mu\text{s}$ , the first-order difference in the average gray intensity of the image drops steadily. However, when the exposure time is greater than 95000  $\mu\text{s}$ , it decreases while there is a certain amount of jitter. In Fig. 7, when the exposure time is between 34200  $\mu\text{s}$  and 95000  $\mu\text{s}$ , the second-order difference of image average gray intensity basically shows a horizontal line, although it fluctuates slightly, while when the exposure time is greater than 95000  $\mu\text{s}$ , the second-order difference of image average gray intensity has relatively large fluctuations. With increasing exposure time, low reflectivity targets can be imaged better. When the exposure time is 380000  $\mu\text{s}$ , a peak appears in the first-order difference curve of image average gray intensity vs. exposure time, as shown in Fig. 6. This means that the average gray

intensity of the image has a relatively sharp change at approximately 380000  $\mu\text{s}$ . According to the above analysis, the exposure time intervals for two targets with different materials were determined to be [34000, 95000] and [380000, 500000], respectively. It should be noted that the first exposure time is rounded off appropriately to make calculation more convenient.

Then, the above two exposure time intervals were divided into several segments, and multiple images were accordingly collected and fused. The areas with different materials of chips in the fused image are clear. A camera parameter, defined to be the product of exposure time and gain, was used to reasonably determine the segmentation. According to the optimal gain determined by the orthogonal experiments and the exposure times determined by the peak of the information entropy vs. exposure time curve, the camera parameters for two material targets are 136800 and 2000000, respectively. Compared with imaging objects with high reflectivity materials, the camera parameter should be larger when imaging objects with low reflectivity materials. Accordingly, the segmentation of the interval [34000, 95000] should be much smaller than that of the interval [380000, 500000]. Consequently, the former interval was divided into 20 subintervals, and the latter interval was divided into 10 subintervals. The segmentation of the former interval is 3100 $\mu\text{s}$  and that of the latter interval is 12000  $\mu\text{s}$ .

## VI. EXPERIMENTS RESULTS AND DISCUSSION

Thirty multi-exposure images were collected with the machine vision system shown in Fig. 3. During image acquisition, the previously determined optimal exposure parameters were adopted. The proposed multi-exposure image processing algorithm was implemented by using MATLAB® 2015. An ordinary PC with a 64-bit operating system was used as an image processing system. Some collected images are included in Table VI.

TABLE VI. SOURCE IMAGES WITH DIFFERENT EXPOSURE TIMES

Images	Exposure times ( $\mu\text{s}$ )	Descriptions
	45000	The pins can be imaged, but the brightness is slightly dark. The characters are completely invisible.
	85000	The pins are incomplete and the characters are still invisible.
	400000	The pins are missing and the characters are visible.

### A. Subjective Evaluation

The information entropy method, window segmentation method and the proposed joint method were employed to fuse the images, and the results are shown in Fig. 8.

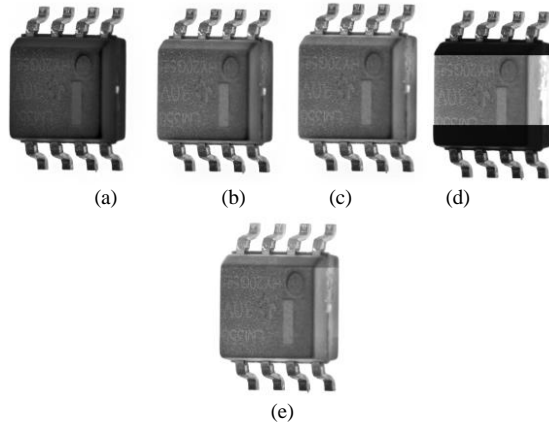


Fig. 8. Results of image fusion. (a) image fusion result based on the Laplacian pyramid strategy with  $\sigma = 0.1$ ; (b) image fusion result based on the Laplacian pyramid strategy with  $\sigma = 0.2$ ; (c) image fusion result based on the Laplacian pyramid strategy with  $\sigma = 0.3$ ; (d) image fusion result based on ordinary window segmentation; (e) image fusion result based on the proposed joint method

Fig. 8(a) to 8(c) show the image fusion results based on the Laplacian pyramid strategy. From the perspective of character clarity, the characters on the plastic package in Fig. 8(a) are very vague. The clarity of characters on the plastic package in Fig. 8(b) is obviously improved compared with that of Fig. 8(a). Compared with Fig. 8(a) and Fig. 8(b), the characters on the plastic package in Fig. 8(c) are the clearest. From the perspective of the pin area contrast, the pin area in Fig. 8(b) has the highest contrast. Fig. 8(d) is the result of image fusion based on window segmentation. Although the contrast of the pin area is high and the characters are relatively clear, there is an obvious "fracture" trace in the fused image, which will cause relatively large interference in subsequent image processing and thus may easily cause measurement errors. Fig. 8(e) is the image fusion result based on the proposed joint method. The characters are clear, the pin area contrast is high, the "fracture" trace is significantly eliminated, the details are well protected, and the visual effect is good.

### B. Objective Evaluation

The above image fusion results were quantitatively analyzed and compared by using three indices, namely, information entropy, average gray intensity and time consumption. The results are tabulated in Table VII.

According to Table VII, in image fusion based on the Laplacian pyramid strategy, the value of  $\sigma$  will affect the information entropy and average gray intensity of the fused image, while it has little impact on the image fusion efficiency. When  $\sigma = 0.1$ , the information entropy of the fused image is 6.1473, and the average gray intensity of the fused image is 89.9575. Compared to  $\sigma = 0.1$ , when  $\sigma = 0.2$ , the information entropy of the fused image increases by 1.27%, and the average gray intensity of the fused image increases by 33.65%. Compared to  $\sigma = 0.1$ , when  $\sigma = 0.3$ , the information entropy of

the fused image increases by 2.12%, and the average gray intensity of the fused image increases by 38.09%.

TABLE VII. OBJECTIVE INDICATORS OF DIFFERENT FUSION RESULTS

Fusion Method	Information Entropy	Average Gray Intensity	Time (s)
Laplace pyramid strategy with $\sigma = 0.1$	6.1473	89.9575	6.246965
Laplace pyramid strategy with $\sigma = 0.2$	6.2252	120.2241	6.245941
Laplace pyramid strategy with $\sigma = 0.3$	6.2778	124.2241	6.220413
Ordinary window segmentation	<b>6.4937</b>	117.4303	5.112153
Proposed method	6.2922	<b>131.5629</b>	<b>4.967878</b>

Image fusion based on window segmentation has the largest information entropy, which is 5.63% higher than the minimum value. However, the average gray intensity of the fused image is not high, ranking fourth (penultimate). The efficiency of the fusion algorithm is improved. Compared with the three image fusion methods based on the Laplacian pyramid strategy, the efficiency of the algorithm is increased by 22.20%, 22.18 % and 21.68%.

Image fusion based on the proposed joint method has higher information entropy, which is better than the three image fusion methods based on the Laplacian pyramid strategy and second to the image fusion method based on window segmentation. The average gray intensity of the fused image is the highest. Compared with the other four methods, the average gray intensity is increased by 46.25%, 9.43%, 5.91% and 12.03%. The fusion algorithm takes the least time. Compared with the image fusion method based on the Laplacian pyramid strategy, it takes approximately 1.3 seconds less. Compared with the image fusion method based on window segmentation, the efficiency of the algorithm is also improved, and this algorithm takes 2.90% less time.

## VII. CONCLUSIONS

To address the difficulty of acquiring high-quality images with single imaging for chips made of two materials with extremely different reflectivity, an image enhancement method based on multi-exposure image fusion was proposed in this paper. First, a joint image fusion algorithm based on the Laplacian pyramid and window segmentation was proposed, improving image quality and reducing processing time. Then, the factors that affect the imaging quality their levels were analyzed and the imaging parameters were optimized through orthogonal tests. After that, a method of determining the exposure time based on information entropy and first and second order difference of average gray intensity was studied. Finally, multi-exposure image sets were established, and experiments and subjective and objective evaluations were subsequently performed. The results show that the fused image has a good visual effect, its information entropy was 6.29, and its average gray intensity was 131.56. Furthermore, compared with the Laplace pyramid strategy, the time consumed was averagely reduced by 1.26 s. The fusion algorithm has the advantages of being less time consuming and high efficiency.

It has been demonstrated that the image enhancement method based on multi-exposure image fusion proposed in this paper is effective for an imaging object composed of two materials with great difference in reflectivity. However, obtaining high-quality images is not the ultimate goal, and it is necessary to further verify the effectiveness of the method in a defect detection or size measurement task. Furthermore, the proposal can be further explored and applied to the objects composed of more than two kinds of materials. On the other hand, although the proposed algorithm takes the shortest time in the above experiments, the image fusion process still takes 4.6 s. So the efficiency should be further improved.

#### ACKNOWLEDGMENT

All authors express their gratitude to the Editor and the anonymous Reviewers for their valuable and constructive comments. And this research was funded by the National Natural Science Foundation of China under grant number 51705238, the Promotion Project for Modern Agricultural Machinery Equipment and Technology Demonstration of Jiangsu Province under grant number NJ2021-58 and Postgraduate Research & Practice Innovation Program of Jiangsu under grant number SJCX21-0913.

#### REFERENCES

- [1] Wang, S.; Wang, H.; Yang, F.; Liu, F.; Zeng, L. Attention-based deep learning for chip-surface-defect detection. *Int.J.Adv.Manuf.Tech.* **2022**, *121*, 1957-1971.
- [2] Kapil Joshi; Manoj Diwakar; Joshi, N.K.; Lamba, S. A Concise Review on Latest Methods of Image Fusion. *Recent advances in computer science and communications* **2021**, *14*, 2046-2056.
- [3] Lapray, P.-J.; Heyrman, B.; Ginhac, D. HDR-ARtiSt: an adaptive real-time smart camera for high dynamic range imaging. *Journal of Real-Time Image Processing* **2016**, *12*, 747-762.
- [4] Zhuang, P.; Ding, X. Correction to: Underwater image enhancement using an edge-preserving filtering Retinex algorithm. *Multimed Tools Appl* **2020**, *79*, 1729.
- [5] Vijayalakshmi, D.; Nath, M.K.; Acharya, O.P. A Comprehensive Survey on Image Contrast Enhancement Techniques in Spatial Domain. *Sensing and Imaging* **2020**, *21*, 40.
- [6] Celik, T. Spatial entropy-based global and local image contrast enhancement. *IEEE Trans Image Process* **2014**, *23*, 5298-5308.
- [7] Enesi, I.; Çiço, B.; Harizaj, M. Increasing quality in fingerprint images by Implementing wavelet transform based fusion technique. *Association for Computing Machinery* **2021**, 112-117.
- [8] Zhang Z; Xu Y; Yang J. A Survey of Sparse Representation: Algorithms and Applications. *IEEE Access*, **2017**, 3:490-530.
- [9] Vivone G ; Alparone L ; Chanussot J. A Critical Comparison Among Pansharpening Algorithms. *IEEE Transactions on Geoenvironment & Remote Sensing*, **2015**, 53(5), 2565-2586.
- [10] Ma, Z.; Oh, C. A Wavelet-Based Dual-Stream Network for Underwater Image Enhancement. In Proceedings of the ICASSP 2022 - 2022 IEEE International Conference on Acoustics, Speech and Signal Processing (ICASSP), **2022**; pp. 2769-2773.
- [11] Fu Z ; Zhu H; Yu S. Multi exposure HDR Image Reconstruction Based on Gray Scale Mapping Function Modeling. *Journal of Data Acquisition and Processing*, **2019**.
- [12] Wang, C.; He, C.; Xu, M. Fast exposure fusion of detail enhancement for brightest and darkest regions. *The Visual Computer* **2021**, *37*, 1233-1243.
- [13] Ma K; Hui L; Yong H. Robust Multi-Exposure Image Fusion: A Structural Patch Decomposition Approach. *IEEE Transactions on Image Processing*, **2017**, 26(5), 2519-2532.
- [14] Lyu, Q.; KinTak, U. A Multi-focus Image-fusion Scheme Based on non-Uniform Triangular Partition. *International Conference on Information Communication and Networks* **2019**, 191-195.
- [15] P, R.T.; D, R. A Hybrid Method for Block-Based Feature Level Image Fusion Technique of PAN and MS Image Using Contourlet Transform with Neural Network. *Journal of Emerging Technologies and Innovative Research* **2019**.
- [16] Hua K L; Wang H C; Yeh C H. Background Extraction Using Random Walk Image Fusion. *IEEE Trans Cybern*, 2018,1-13.
- [17] Singh, S.; Mittal, N.; Singh, H. Review of Various Image Fusion Algorithms and Image Fusion Performance Metric. *Archives of Computational Methods in Engineering* **2021**, *28*, 3645-3659.
- [18] Vanmali, A.V.; Gadre, V.M. Visible and NIR image fusion using weight-map-guided Laplacian-Gaussian pyramid for improving scene visibility. *Sādhanā* **2017**, *42*, 1063-1082.
- [19] Qu, Z.; Huang, X.; Liu, L. An improved algorithm of multi-exposure image fusion by detail enhancement. *Multimedia Systems* **2021**, *27*, 33-44.
- [20] Turgut S S ; Oral M. Multi-Focus Image Fusion based on Gradient Transform. *Computer Vision and Pattern Recognition*, **2022**.
- [21] Kataoka K, Kameda Y, Hamamoto T. Adaptive Exposure-time Control Based on Image Entropy for Multiple-exposure-time Image Sensor. *ITE Transactions on Media Technology and Applications*, 2021, 9(2):128-135.
- [22] Zhang W, Sun X, Yu Q. Fast Exposure Fusion Based on Camera Response Function. *DEStech Transactions on Computer Science and Engineering*, 2020.
- [23] X. Deng; Y. Zhang; M. Xu; S. Gu and Y. Duan. Deep Coupled Feedback Network for Joint Exposure Fusion and Image Super-Resolution, *IEEE Transactions on Image Processing* **2021**, *30*, 3098-3112.